

Fluid Dynamics Network: Topology-Agnostic 4D Reconstruction via Fluid Dynamics Priors

Daniele Baieri
Sapienza University of Rome
baieri@di.uniroma1.it

Stefano Esposito
Hochschule Bonn-Rhein-Sieg
stefano.esposito@h-brs.de

Filippo Maggioli
Sapienza University of Rome
maggioli@di.uniroma1.it

Emanuele Rodolà
Sapienza University of Rome
rodola@di.uniroma1.it

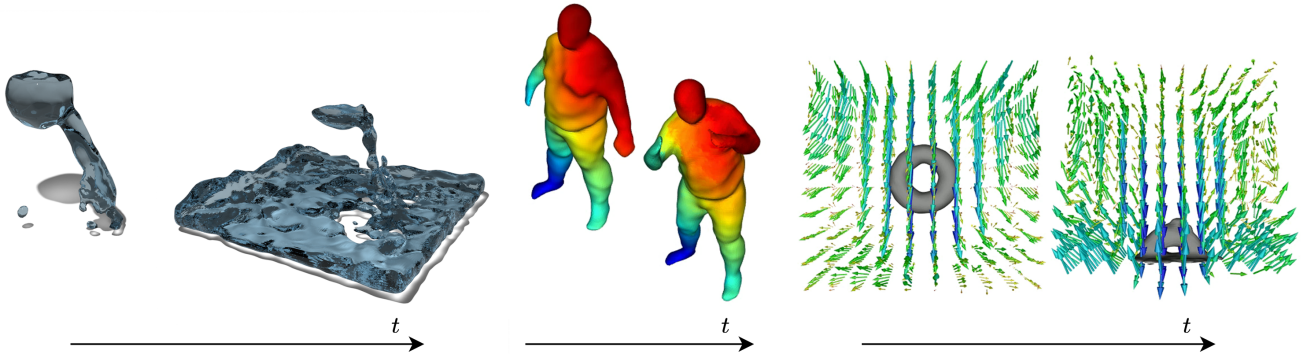


Figure 1: Left: simulation of a fluid dynamic reconstructed with our method. Middle: a correspondence on a humanoid character induced by our model. Right: a 3D object and the deformation velocity field reconstructed with our method.

Abstract

Representing 3D surfaces as level sets of continuous functions over \mathbb{R}^3 is the common denominator of neural implicit representations, which recently enabled remarkable progress in geometric deep learning and computer vision tasks. In order to represent 3D motion within this framework, it is often assumed (either explicitly or implicitly) that the transformations which a surface may undergo are homeomorphic: this is not necessarily true, for instance, in the case of fluid dynamics. In order to represent more general classes of deformations, we propose to apply this theoretical framework as regularizers for the optimization of simple 4D implicit functions (such as signed distance fields). We show that our representation is capable of capturing both homeomorphic and topology-changing deformations, while also defining correspondences over the continuously-reconstructed surfaces.

1. Introduction

Representing the motion of 3D objects is a crucial aspect in several areas of 3D graphics. For instance, skinning models are an established method for mesh animation, which provides a plausible and efficient way of deforming a surface given a sequence of skeleton poses [19]. However, various applications such as fluid simulation require representing topology-changing (formally, non-homeomorphic) deformations, which are notoriously difficult to approach with mesh-based approaches.

Implicit representations are becoming an increasingly important topic in computer graphics, as they enable or improve a variety of game-changing technologies, such as shape modeling [30], accurate shape and scene reconstruction [15, 33] and fast rendering [12, 16, 34]. Yet, the representation of a 3D object with a signed distance field introduces many challenges since many established pipelines from classical computer graphics cannot be applied anymore. Between these challenges, the non-rigid animation of a body is one of the most obvious, as standard approaches

like skinning models do not have straightforward conversions for working with implicit representations.

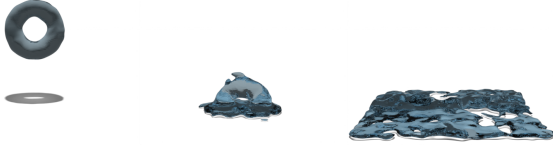


Figure 2: Frames from a simulation reconstructed with our framework. The model is able to capture the drastic topological changes in the deformed geometry.

Recently, some works presented significant progresses in this direction. Taking advantage of deep learning techniques, it has been shown that implicit surfaces can be successfully rigged and animated using skeletons, with a particular focus on humanoid characters [9, 47]. Other approaches got rid of skeletal animations and focused on reconstructing 3D geometries that are continuously deformed over time from a set of discrete observations [25, 36]. However, these techniques represent deformation as continuous bijective functions with continuous inverse, and as a consequence they are limited to representing fixed-topology deformations.

We fill this gap by introducing a new computational model that can reconstruct continuously deformable 3D objects from a discrete sample of observations without any assumptions on the topology changes. Our approach is shown to be effective in settings where the geometry deformation is homeomorphic (such as character animations), as well as applications where the topology changes drastically over time (like fluid dynamics scenes). We also show that the 4D reconstruction produced by our model can be used to track dense correspondences in the evolving surface, making it also suitable for shape-matching applications.

2. Related work

Neural implicit representations Representing 3D surfaces as continuous functions over ambient space is a recent trend in geometric deep learning. Manipulating continuous surfaces offers new perspectives in geometry processing, and led to significant advances in various complex tasks. Occupancy fields [32] and signed distance fields [38] were applied in several different settings, such as 3D surface reconstruction [1, 15, 40, 43, 52], animation [9, 47], and inverse rendering [35, 37, 55]. This last application was revolutionized by neural radiance fields [33], which inspired an entire line of research. Successively, NeRFs were applied to deforming scenes (4D reconstruction from multi-view videos) [10, 39, 41, 48], MRI scans [11, 31], and for scene relighting [5, 44, 56]. Instant-NGP [34] further enabled application of neural implicit representations by showing how to optimize them in a matter of seconds.

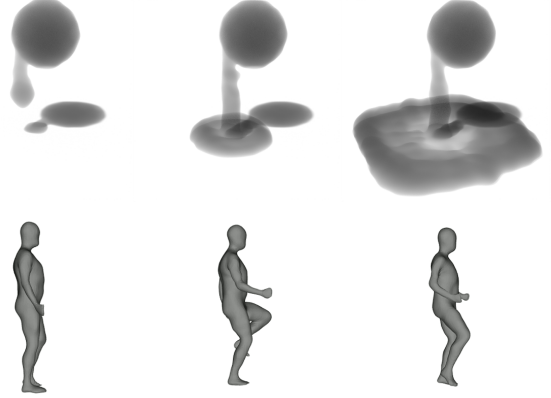


Figure 3: Our neural implicit representation can infer the dynamics of complex fluid simulation scenes (left) and simpler human body animations (right) with a unified formulation, while defining correspondences among the reconstructed surfaces.

4D shape reconstruction Continuous 4D reconstruction methods tackle the reconstruction of dynamic scenes both in space and time from a sequence of sparse observations, typically point-clouds or 2D images. While 3D reconstruction allows for several algorithmic baselines (such as [8, 21]), the complexity introduced by the requirement of reconstructing motion steered this task towards deep learning methods, and most recently, neural implicit representations.

PSGN [13] is a 3D reconstruction method for multi-view images which can be easily generalized to predict a 4D point cloud, i.e. the point cloud trajectory instead of a single point set. Similarly, implicit representation networks such as occupancy net [32] can be generalized by adding an input coordinate (usually called ONet4D), in order to define the occupancy field in the spatio-temporal domain by predicting time-varying occupancy values. By assigning a velocity vector to every point in space and time, Niemeyer *et al.* [36] offered a method to represent continuous 4D shapes by transporting a static occupancy field, while also implicitly modeling dense correspondences. Tang *et al.* [46] proposed a novel 4D point cloud encoder design that performs efficient spatio-temporal shape properties aggregation from 4D point cloud sequences, improving upon Occupancy Flow’s reconstructed geometry. CaDeX [25] explicitly represents the deformation as an homeomorphism, by factorizing it into a continuous invertible function and its continuous inverse, mapping the source geometry frame into a common 3D coordinate space and back to the destination frame, respectively; its prior allows for topology preservation by construction and the recovery of consistent correspondences across frames.

All aforementioned methods are data driven, where at

test time reconstructions are conducted from an image or a partial observations leveraging prior knowledge learned from large-scale datasets containing both complete surfaces (*i.e.* meshes) and their sparse observations. This improves the accuracy and consistency of the results, especially in situations where the input data is noisy or incomplete. However, prior-based methods can be computationally expensive and their large amounts of training data requirement can limit their practical applicability.

Furthermore, a common assumption among these methods is preservation of topology; for instance, the integration of points through the velocity field learned by Occupancy Flow is also implicitly an homeomorphism. Our method will make no such assumption, thus retaining an additional level of generality, and can be optimized from a sequence of dense oriented point clouds, without data priors.

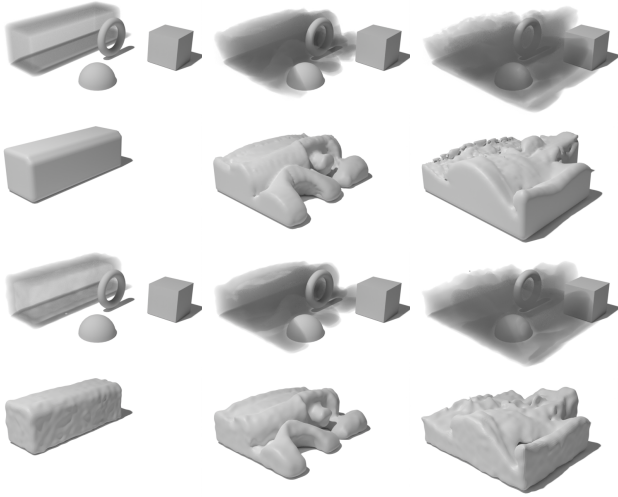


Figure 4: The simulation of a cold gas in a scene containing obstacles (1st row) and the geometry surrounding the volume (2nd row), compared with the reconstruction obtained with our framework (3rd row) and the reconstructed mesh (4th row). Our method is able to capture the complex behaviour of the gas moving around the obstacles in the scene.

Computational fluid dynamics The simulation of fluid dynamics is a fundamental topic in computer graphics, and much research has been devoted to this area in the last decades. Researchers have approached this problem from a variety of points of view, spanning from the direct simulation of Navier-Stokes equations [7] to non physics-based algorithm for credible visual results [14, 17]. For a detailed survey on fluid solvers, we refer to Bridson’s textbook [6] and Koshier *et al.* [23]. Despite the amount of work dedicated to this problem, the room for improvement is still significant, and new studies on fluid simulation are continuously coming out. In recent years, many studies tried to

achieve better quality in simulation by focusing on specific problems, like certain kinds of waves [18] and particular environmental conditions [24]. Simultaneously, new techniques for speeding up simulations have been developed, with particular attention to the interaction between solid obstacles and turbulent fluids [26, 29] and to efficient space partitioning [42].

Machine learning and fluid simulation Recently, more innovative approaches tried to combine the descriptive power of machine learning with the simulation of fluid dynamics. Um *et al.* showed a general method to improve PDE solvers (such as fluid simulators) solutions using statistical ML models [49]. Vinuesa *et al.* [51] tried to apply learning paradigms to different stages of fluid simulation, showing the potential improvement in quality and performance. Following this direction, data-driven models have been developed for upsampling turbulent flows and obtaining fine-grained details from coarse simulations [2, 3]. Fluid super-resolution has also been tackled in a GAN paradigm, as in [53, 54]. A completely different approach has been proposed in Li *et al.* [27], where particle-based fluid models have successfully been related to graph neural networks obtaining performance improvement at basically no quality cost. Ummenhofer *et al.* [50] later showed that the same can be achieved without graph structure, by performing continuous convolution over sets of points. More similar in spirit to our work is Chu *et al.* [10]: the authors apply fluid simulation priors to inverse rendering of dynamic fluid scenes from sparse multi-view videos, without geometric information.

3. Method

3.1. Preliminaries

Simulating fluid dynamics typically involves computing a velocity field \mathbf{u} , by integrating the Navier-Stokes PDE:

$$\frac{\partial \mathbf{u}}{\partial t} + (\mathbf{u} \cdot \nabla) \mathbf{u} - \nu \nabla^2 \mathbf{u} = -\frac{1}{\rho} \nabla p + \mathbf{g} \quad (1)$$

$$\nabla \cdot \mathbf{u} = 0 \quad (2)$$

And applying the resulting velocity field \mathbf{u} to transport some type of geometric representation. For our purposes, we represent geometry as a scalar field f , which can be transported via the advection equation (assuming eq. (2) holds):

$$\frac{\partial f}{\partial t} + \mathbf{u} \cdot \nabla f = 0 \quad (3)$$

Typically, simulators will integrate a simpler form of Eq. 1, only enforcing self-advection:

$$\frac{\partial \mathbf{u}}{\partial t} + (\mathbf{u} \cdot \nabla) \mathbf{u} = 0 \quad (4)$$

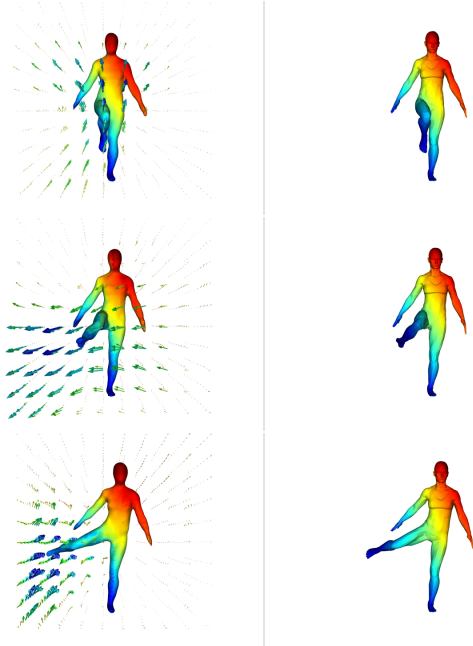


Figure 5: An animation from the D-FAUST dataset (right) compared with the reconstruction obtained with our model (left). The colormap shows the preservation of correspondences established by the velocity function along the deformation.

and add on top of this partial result the effects of pressure (p), external forces (\mathbf{g}) and viscosity ($\nabla^2 \mathbf{u}$), which are solved for independently. This approximation mitigates the complexity of integrating Eq. (1) while retaining high precision. In a similar spirit, we use Eq. (4) as a structural prior and allow our model to estimate the influence of the aforementioned components from the data.

3.2. Regularizing 4D reconstruction by CFD priors

Our method leverages fluid simulation priors as a regularizer for the optimization of a neural representation of the 4D geometry and dynamics. Let $f_\theta: \mathbb{R}^4 \rightarrow \mathbb{R}^d$, $v_\phi: \mathbb{R}^4 \rightarrow \mathbb{R}^3$ be our (temporal) geometry and velocity functions, represented as neural networks. As outlined by Niemeyer *et al.* in [36], a trivial solution to the 4D reconstruction task can be found by optimizing the general loss:

$$\mathcal{L}_{\text{recon}} = \sum_{t \in T} L(f_\theta, \mathcal{X}_t; \tau(t)) \quad (5)$$

Where $\{\mathcal{X}_t\}_{t \in T}$ are time-labeled sparse geometry observations, T is the set of available supervised time steps, τ maps a timestep label to a real time value, and L is an error function comparing the optimized function and the ground truth data.

This model (DeepSDF4D in the following), while technically correct, does not learn any information about the

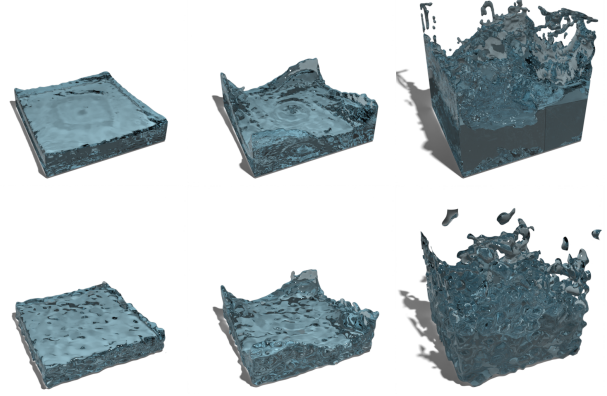


Figure 6: Real simulation of a swirling fluid (top) compared with the reconstruction obtained with our method (bottom). The fluid dynamics priors given to the model allow for catching the complexity in the deformation.

dynamics underlying the observations; thus, it is similar to applying a 3D reconstruction technique for each frame. As a consequence, no type of correspondence among reconstructed surfaces is established during training. Despite these shortcomings, however, it allows to represent general deformations of 3D geometry, including topological and volume changes. Most proposals in 4D reconstruction literature (such as [25, 36]) rule this possibility out by assuming to only work with isometries (either implicitly or explicitly); we discuss how to improve DeepSDF4D in order to model general deformations (up to volume changes), while establishing correspondences between the reconstructed surfaces.

Similarly to Chu *et al.* [10], we train v_ϕ jointly with f_θ using the following losses, adapted from Eqs. (2) to (4):

$$\mathcal{L}_{\text{div}} = \int_0^\tau \int_{\mathbb{R}^3} \nabla \cdot v_\phi d\mathbf{x} dt \quad (6)$$

$$\mathcal{L}_{\text{advect}} = \int_0^\tau \int_{\mathbb{R}^3} \frac{\partial f_\theta}{\partial t} + v_\phi \cdot \nabla f_\theta d\mathbf{x} dt \quad (7)$$

$$\mathcal{L}_{\text{NS}} = \int_0^\tau \int_{\mathbb{R}^3} \frac{\partial v_\phi}{\partial t} + (v_\phi \cdot \nabla) v_\phi d\mathbf{x} dt \quad (8)$$

Where $\mathcal{L}_{\text{advect}}$ is only used to train v_ϕ (otherwise it is trivially minimized by zeroing f_θ). We discuss how we approximate these integrals in Sec. 3.3.2.

While Eq. (7) is enough to optimize v_ϕ with respect to a given set of observations (assuming f_θ is also trained via Eq. (5)), we still need to regularize our geometry function based on our learned velocity field. An option is to perform random linear warping, as in [10, 48]: that is, we query our geometry network for points \mathbf{x} at a given timestep t_i as

$$\hat{f}_\theta(\mathbf{x}, t_i) = f_\theta(\mathbf{x} + \delta_t v_\phi(\mathbf{x}, t_i), t_i + \delta_t) \quad (9)$$

For randomly sampled δ_t (further discussion about sampling in Sec. 3.3.2). In combination with Eq. (5), linear warping allows to transport supervision signals across time through v_ϕ . Finally, we instantiate $\mathcal{L}_{\text{recon}}$ as a SDF reconstruction loss, similar to Park *et al.* [38]:

$$L(f_\theta, \mathcal{X}_t; \tau(t)) = \int_{\mathbb{R}^3} \|f_\theta(\mathbf{x}, \tau(t)) - d(\mathbf{x}, \mathcal{X}_t)\| d\mathbf{x} \quad (10)$$

Where $\{\mathcal{X}_t\}_{t \in T}$ are oriented point clouds, and d computes the ground-truth signed distance value for \mathbf{x} by mapping it to the closest point \mathbf{p} on \mathcal{X}_t and determining its sign (inside/outside) via the winding number of \mathbf{p} [20].

3.3. Implementation details

3.3.1 Model

We implement f_θ and v_ϕ as two Siren [43] networks with 5 layers and 256 hidden units. We find that the high-frequency bias induced by this architecture is really beneficial in learning erratic and unpredictable dynamics such as fluid behaviour, allowing to considerably speed up convergence and properly model surface details. Figure 7 highlights this aspect by comparing Siren with a simple MLP with positional encoding [45]. Our networks are trained with the loss function

$$\mathcal{L} = \mathcal{L}_{\text{recon}} + \lambda_1 \mathcal{L}_{\text{div}} + \lambda_2 \mathcal{L}_{\text{advect}} + \lambda_3 \mathcal{L}_{\text{NS}} \quad (11)$$

Where we set $\lambda_1 = \lambda_2 = 10, \lambda_3 = 0.1$.

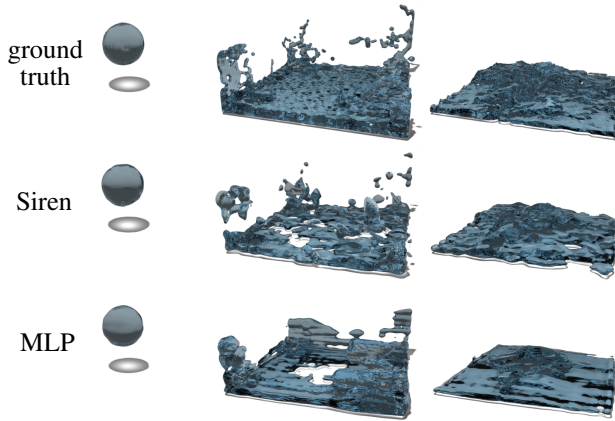


Figure 7: Frames from a simulation obtained using the Siren networks (middle) compared with Softplus-activated MLPs (bottom). The former is able capture higher frequency details, producing surface displacements typical of moving fluids, and better matching the reference simulation (top).

3.3.2 Training

Our networks are trained for 500 epochs using the Adam optimizer [22] with a learning rate of $1e-4$. During each

training iteration, we need to approximate the integrals in our loss functions (Eqs. (6) to (8) and (10)). We approximate the time integral via stratified sampling, similarly to how Mildenhall *et al.* [33] integrate radiance and density to compute light transport on a single ray. Over multiple epochs, this helps to retain continuity of the representation over time (as opposed to, *e.g.*, always integrating over a fixed linear space of time steps). Therefore, we evaluate our loss functions independently for each time step and sum all the loss gradients before updating network parameters. For each timestep, the space integral is approximated by uniformly sampling in a bounding box D .

Training occurs in three phases: first, we train f_θ to near convergence over the input data. Then, based on the partial solution provided by f_θ , we train the velocity network v_ϕ by the fluid dynamics priors encoded in Eqs. (6) to (8). During the last phase, we introduce linear warping with a linear schedule, *i.e.*, the interval from which we uniformly sample δ_t to compute Eq. (9) grows linearly with training time, up to the entire space between adjacent supervised frames. We find that running each phase for 200 epochs yields satisfying results.

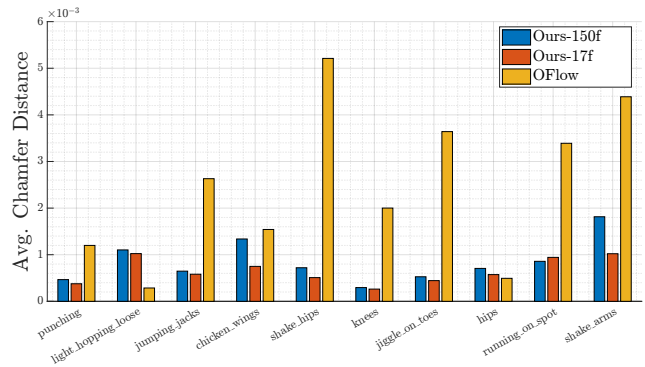


Figure 8: Evaluation of reconstruction quality of our method on a subset of the DFAUST dataset (lower is better). OFlow and Ours-17f are evaluated on the first 17 frames of each sequence. While the high frequency of our geometry function may hinder reconstruction quality to a small degree, our method manages to reconstruct dynamics more faithfully than Occupancy Flow.

4. Experiments

4.1. 4D surface reconstruction

In order to measure the representational power of our method, we compare meshes extracted from our method using marching cubes [28] with resolution 128 against ground-truth meshes, using the chamfer distance as metric. We run the evaluation over a small subset of the DFAUST dataset [4], where we select one sequence type for each subject, so that most of the sequence types are represented.

The results are showed in Figure 8.

4.2. Shape correspondence

Our method defines a temporal velocity field, which we may leverage in order to define correspondences among the reconstructed surfaces. Furthermore, by relaxing assumptions on the deformation function, we model correspondences with changes of topology (*e.g.* Figure 10) in a fully unsupervised fashion. Formally, for a single sequence of observations $\{\mathcal{X}_i\}_{i=1}^n$, we define the correspondence between the vertices of \mathcal{X}_1 and \mathcal{X}_n via the initial value problem:

$$\begin{aligned}\Phi(\mathcal{X}_1, 0) &= \mathcal{X}_1 \\ \dot{\Phi}(\mathcal{X}_1, t) &= v_\phi(\mathcal{X}_1, t)\end{aligned}\quad (12)$$

We integrate Φ via Euler using $[\tau(1); \tau(n)]$ as time interval. After flowing a point x through the entire time interval via $\Phi(x, \tau(n))$, we select the result on the target set of vertices as the nearest neighbor

$$\Pi(x) = \underset{z \in \mathcal{X}_n}{\operatorname{argmin}} \|\Phi(x, \tau(n)) - z\|_2 \quad (13)$$

In order to compare our matching method quantitatively to other 4D reconstruction algorithms with correspondences, we plot a comparison in cumulative matching curves evaluated on the same subset of DFAUST described in Sec. 4.1. For each analyzed sequence, we match the first and last frames; then, we take as point-wise error metric the geodesic distance between the ground-truth match and the predicted match. The results are showed in Figure 9. We evaluate our method with subsequences of 150 frames and

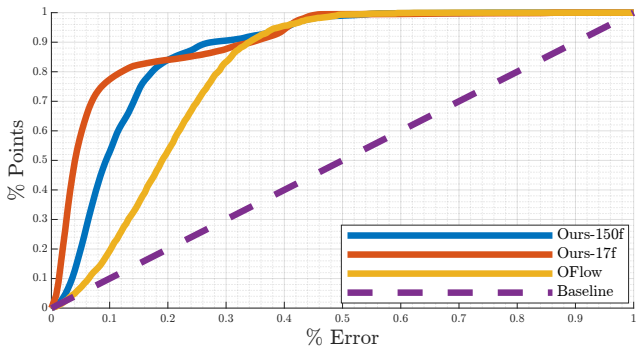


Figure 9: Quantitative comparison of correspondences on DFAUST between our method and Occupancy Flow [36]. Our method manages to match most points with low error (80% of points have error percentage below 10% for the 17 frames evaluation). Saturation seems comparable with the Occupancy Flow pretrained model.

17 frames, in order to compare it to the pretrained Occupancy Flow model, which was trained only on 17 frames sequences.

5. Conclusions

5.1. Discussion and limitations

We presented a non-data-driven method for 4D reconstruction which is capable of capturing a vast range of geometric deformations and define dense, continuous correspondences among the reconstructed surfaces. One main limitation of our method is its requirement for dense input point clouds; we propose to investigate solutions in the future (see Sec. 5.2).

Furthermore, the simplified version of the Navier-Stokes equation which we use in our loss function (Eq. (8)) is not enough to capture any fluid behaviour: imagine a cylinder

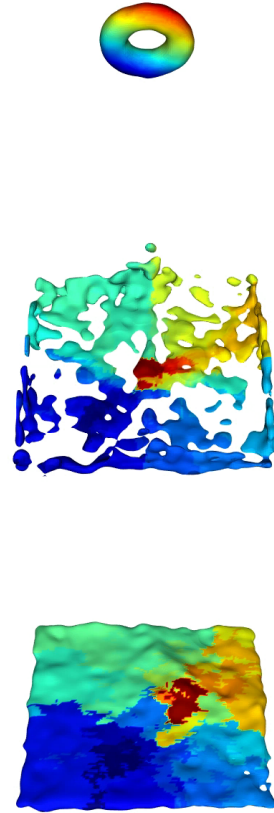


Figure 10: An example of predicted correspondences under dramatic changes of topology. Despite the absence of semantics in vertex identity, the indicator function is preserved coherently with surface dynamics.

rotating on its “up” axis. The ground-truth SDF signal for the sequence of shapes will be constant, and therefore the velocity field regressed by our method will be close to zero everywhere. This setting is also not unlikely in fluid simulation, as it is a close analogy for a vortex of high-viscosity fluid. This issue may be addressed by employing the complete Navier-Stokes form, at the cost of having to regress additional functions (such as pressure and external forces) and to optimize second derivatives of the velocity field. One last limitation would be the case of handling non-volume-preserving deformations; however, the entire fluid simulations framework is unsuited for this purpose, thus we consider it to be outside of our scope.

5.2. Future work

In the near future, we intend to gather the experimental fluid data which we employed for this work into a proper, multimodal (including multi-view renders) 4D geometry dataset. This should provide for a useful benchmark for topology-agnostic methods in geometry processing.

Furthermore, we intend to generalize our presented formulation to a data-driven model: this should allow us to relieve our need for dense geometric input at inference time, albeit constraining the learned model to the distribution presented in the employed dataset.

Lastly, we intend to investigate the capabilities of our formulation in point cloud segmentation, in particular, we believe our method has promise in separating static and dynamic content in 4D point clouds.

References

- [1] Matan Atzmon and Yaron Lipman. SAL: sign agnostic learning of shapes from raw data. In *2020 IEEE/CVF Conference on Computer Vision and Pattern Recognition, CVPR 2020, Seattle, WA, USA, June 13-19, 2020*, pages 2562–2571. IEEE, 2020. [2](#)
- [2] Kai Bai, Wei Li, Mathieu Desbrun, and Xiaopei Liu. Dynamic upsampling of smoke through dictionary-based learning. *ACM Trans. Graph.*, 40(1), sep 2020. [3](#)
- [3] Kai Bai, Chunhao Wang, Mathieu Desbrun, and Xiaopei Liu. Predicting high-resolution turbulence details in space and time. *ACM Trans. Graph.*, 40(6), dec 2021. [3](#)
- [4] Federica Bogo, Javier Romero, Gerard Pons-Moll, and Michael J. Black. Dynamic FAUST: Registering human bodies in motion. In *IEEE Conf. on Computer Vision and Pattern Recognition (CVPR)*, July 2017. [5](#)
- [5] Mark Boss, Raphael Braun, Varun Jampani, Jonathan T Barron, Ce Liu, and Hendrik Lensch. Nerd: Neural reflectance decomposition from image collections. In *Proceedings of the IEEE/CVF International Conference on Computer Vision*, pages 12684–12694, 2021. [2](#)
- [6] R. Bridson. *Fluid Simulation for Computer Graphics*. CRC Press, 2018. [3](#)
- [7] Robert Bridson and Matthias Müller-Fischer. Fluid simulation: Siggraph 2007 course notes video files associated with this course are available from the citation page. SIGGRAPH ’07, page 1–81, New York, NY, USA, 2007. Association for Computing Machinery. [3](#)
- [8] Fatih Calakli and Gabriel Taubin. Ssd: Smooth signed distance surface reconstruction. *Comput. Graph. Forum*, 30(7):1993–2002, 2011. [2](#)
- [9] Xu Chen, Yufeng Zheng, Michael J Black, Otmar Hilliges, and Andreas Geiger. Snarf: Differentiable forward skinning for animating non-rigid neural implicit shapes. In *International Conference on Computer Vision (ICCV)*, 2021. [2](#)
- [10] Mengyu Chu, Lingjie Liu, Quan Zheng, Erik Franz, Hans-Peter Seidel, Christian Theobalt, and Rhaleb Zayer. Physics informed neural fields for smoke reconstruction with sparse data. *ACM Transactions on Graphics*, 41(4):119:1–119:14, aug 2022. [2](#), [3](#), [4](#)
- [11] Abril Corona-Figueroa, Jonathan Frawley, Sam Bond-Taylor, Sarath Bethapudi, Hubert P. H. Shum, and Chris G. Willcocks. Mednerf: Medical neural radiance fields for reconstructing 3d-aware ct-projections from a single x-ray, 2022. [2](#)
- [12] Stefano Esposito, Daniele Baieri, Stefan Zellmann, André Hinkenjann, and Emanuele Rodolà. Kiloneus: A versatile neural implicit surface representation for real-time rendering, 2022. [1](#)
- [13] Haoqiang Fan, Hao Su, and Leonidas Guibas. A point set generation network for 3d object reconstruction from a single image. pages 2463–2471, 07 2017. [2](#)
- [14] Alain Fournier and William T. Reeves. A simple model of ocean waves. *SIGGRAPH Comput. Graph.*, 20(4):75–84, aug 1986. [3](#)
- [15] Amos Gropp, Lior Yariv, Niv Haim, Matan Atzmon, and Yaron Lipman. Implicit geometric regularization for learning shapes. In *Proceedings of the 37th International Conference on Machine Learning, ICML 2020, 13-18 July 2020, Virtual Event*, volume 119 of *Proceedings of Machine Learning Research*, pages 3789–3799. PMLR, 2020. [1](#), [2](#)
- [16] John C Hart et al. Sphere tracing: Simple robust antialiased rendering of distance-based implicit surfaces. In *SIGGRAPH*, volume 93, pages 1–11, 1993. [1](#)
- [17] Damien Hinsic, Fabrice Neyret, and Marie-Paule Cani. Interactive animation of ocean waves. SCA ’02, page 161–166, New York, NY, USA, 2002. Association for Computing Machinery. [3](#)
- [18] Libo Huang, Ziyin Qu, Xun Tan, Xinxin Zhang, Dominik L. Michels, and Chenfanfu Jiang. Ships, splashes, and waves on a vast ocean. *ACM Transaction on Graphics*, 40(6), 12 2021. [3](#)
- [19] Alec Jacobson, Zhigang Deng, Ladislav Kavan, and J. P. Lewis. Skinning: Real-time shape deformation (full text not available). In *ACM SIGGRAPH 2014 Courses*, SIGGRAPH ’14, New York, NY, USA, 2014. Association for Computing Machinery. [1](#)
- [20] Alec Jacobson, Ladislav Kavan, and Olga Sorkine-Hornung. Robust inside-outside segmentation using generalized winding numbers. 32(4), jul 2013. [5](#)
- [21] Michael Kazhdan, Matthew Bolitho, and Hugues Hoppe. Poisson Surface Reconstruction. In Alla Sheffer and Kon-

- rad Polthier, editors, *Symposium on Geometry Processing*. The Eurographics Association, 2006. 2
- [22] Diederik P. Kingma and Jimmy Ba. Adam: A method for stochastic optimization. In Yoshua Bengio and Yann LeCun, editors, *3rd International Conference on Learning Representations, ICLR 2015, San Diego, CA, USA, May 7-9, 2015, Conference Track Proceedings*, 2015. 5
- [23] Dan Koschier, Jan Bender, Barbara Solenthaler, and Matthias Teschner. Smoothed Particle Hydrodynamics Techniques for the Physics Based Simulation of Fluids and Solids. In Wenzel Jakob and Enrico Puppo, editors, *Eurographics 2019 - Tutorials*. The Eurographics Association, 2019. 3
- [24] Bo Lan, You-Rong Li, Peng-Cheng Li, and Hua-Feng Gong. Numerical simulation of the chimney effect on smoke spread behavior in subway station fires. *Case Studies in Thermal Engineering*, 39:102446, 2022. 3
- [25] Jiahui Lei and Kostas Daniilidis. Cadex: Learning canonical deformation coordinate space for dynamic surface representation via neural homeomorphism. In *Proceedings of the IEEE/CVF Conference on Computer Vision and Pattern Recognition*, 2022. 2, 4
- [26] Wei Li, Yixin Chen, Mathieu Desbrun, Changxi Zheng, and Xiaopei Liu. Fast and scalable turbulent flow simulation with two-way coupling. *ACM Trans. Graph.*, 39(4), aug 2020. 3
- [27] Zijie Li and Amir Barati Farimani. Graph neural network-accelerated lagrangian fluid simulation. *Computers & Graphics*, 103:201–211, 2022. 3
- [28] William E. Lorensen and Harvey E. Cline. Marching cubes: A high resolution 3d surface construction algorithm. *SIGGRAPH Comput. Graph.*, 21(4):163–169, aug 1987. 5
- [29] Chaoyang Lyu, Wei Li, Mathieu Desbrun, and Xiaopei Liu. Fast and versatile fluid-solid coupling for turbulent flow simulation. *ACM Trans. Graph.*, 40(6), dec 2021. 3
- [30] R. Malladi, J.A. Sethian, and B.C. Vemuri. Shape modeling with front propagation: a level set approach. *IEEE Transactions on Pattern Analysis and Machine Intelligence*, 17(2):158–175, 1995. 1
- [31] Shuangming Mao and Seiichiro Kamata. Mri super-resolution using implicit neural representation with frequency domain enhancement. In *Proceedings of the 7th International Conference on Biomedical Signal and Image Processing, ICBIP '22*, page 30–36, New York, NY, USA, 2022. Association for Computing Machinery. 2
- [32] Lars M. Mescheder, Michael Oechsle, Michael Niemeyer, Sebastian Nowozin, and Andreas Geiger. Occupancy networks: Learning 3d reconstruction in function space. In *IEEE Conference on Computer Vision and Pattern Recognition, CVPR 2019, Long Beach, CA, USA, June 16-20, 2019*, pages 4460–4470. Computer Vision Foundation / IEEE, 2019. 2
- [33] Ben Mildenhall, Pratul P. Srinivasan, Matthew Tancik, Jonathan T. Barron, Ravi Ramamoorthi, and Ren Ng. Nerf: Representing scenes as neural radiance fields for view synthesis. In *ECCV*, 2020. 1, 2, 5
- [34] Thomas Müller, Alex Evans, Christoph Schied, and Alexander Keller. Instant neural graphics primitives with a multiresolution hash encoding. *arXiv:2201.05989*, 2022. 1, 2
- [35] Michael Niemeyer, Lars Mescheder, Michael Oechsle, and Andreas Geiger. Differentiable volumetric rendering: Learning implicit 3d representations without 3d supervision. In *Proc. IEEE Conf. on Computer Vision and Pattern Recognition (CVPR)*, 2020. 2
- [36] Michael Niemeyer, Lars M. Mescheder, Michael Oechsle, and Andreas Geiger. Occupancy flow: 4d reconstruction by learning particle dynamics. In *2019 IEEE/CVF International Conference on Computer Vision, ICCV 2019, Seoul, Korea (South), October 27 - November 2, 2019*, pages 5378–5388. IEEE, 2019. 2, 4, 6
- [37] Michael Oechsle, Songyou Peng, and Andreas Geiger. Unisurf: Unifying neural implicit surfaces and radiance fields for multi-view reconstruction. In *Proceedings of the IEEE/CVF International Conference on Computer Vision*, pages 5589–5599, 2021. 2
- [38] Jeong Joon Park, Peter Florence, Julian Straub, Richard A. Newcombe, and Steven Lovegrove. Deepsdf: Learning continuous signed distance functions for shape representation. In *IEEE Conference on Computer Vision and Pattern Recognition, CVPR 2019, Long Beach, CA, USA, June 16-20, 2019*, pages 165–174. Computer Vision Foundation / IEEE, 2019. 2, 5
- [39] Keunhong Park, Utkarsh Sinha, Jonathan T. Barron, Sofien Bouaziz, Dan B Goldman, Steven M. Seitz, and Ricardo Martin-Brualla. Nerfies: Deformable neural radiance fields. *ICCV*, 2021. 2
- [40] Songyou Peng, Michael Niemeyer, Lars Mescheder, Marc Pollefeys, and Andreas Geiger. Convolutional occupancy networks. In *European Conference on Computer Vision (ECCV)*, 2020. 2
- [41] Albert Pumarola, Enric Corona, Gerard Pons-Moll, and Francesc Moreno-Noguer. D-nerf: Neural radiance fields for dynamic scenes, 2020. 2
- [42] Han Shao, Libo Huang, and Dominik L. Michels. A fast unsmoothed aggregation algebraic multigrid framework for the large-scale simulation of incompressible flow. *ACM Transaction on Graphics*, 41(4), 07 2022. 3
- [43] Vincent Sitzmann, Julien N.P. Martel, Alexander W. Bergman, David B. Lindell, and Gordon Wetzstein. Implicit neural representations with periodic activation functions. In *arXiv*, 2020. 2, 5
- [44] Pratul P. Srinivasan, Boyang Deng, Xiuming Zhang, Matthew Tancik, Ben Mildenhall, and Jonathan T. Barron. Nerv: Neural reflectance and visibility fields for relighting and view synthesis. In *CVPR*, 2021. 2
- [45] Matthew Tancik, Pratul P. Srinivasan, Ben Mildenhall, Sara Fridovich-Keil, Nithin Raghavan, Utkarsh Singhal, Ravi Ramamoorthi, Jonathan T. Barron, and Ren Ng. Fourier features let networks learn high frequency functions in low dimensional domains. *NeurIPS*, 2020. 5
- [46] Jiapeng Tang, Dan Xu, Kui Jia, and Lei Zhang. Learning parallel dense correspondence from spatio-temporal descriptors for efficient and robust 4d reconstruction. In *Proceedings of the IEEE/CVF Conference on Computer Vision and Pattern Recognition*, pages 6022–6031, 2021. 2
- [47] Garvita Tiwari, Nikolaos Sarafianos, Tony Tung, and Gerard Pons-Moll. Neural-gif: Neural generalized implicit func-

- tions for animating people in clothing. In *International Conference on Computer Vision (ICCV)*, 2021. 2
- [48] Edgar Tretschk, Ayush Tewari, Vladislav Golyanik, Michael Zollhöfer, Christoph Lassner, and Christian Theobalt. Non-rigid neural radiance fields: Reconstruction and novel view synthesis of a dynamic scene from monocular video, 2020. 2, 4
 - [49] Kiwon Um, Robert Brand, Yun (Raymond) Fei, Philipp Holl, and Nils Thuerey. Solver-in-the-loop: Learning from differentiable physics to interact with iterative pde-solvers. In H. Larochelle, M. Ranzato, R. Hadsell, M.F. Balcan, and H. Lin, editors, *Advances in Neural Information Processing Systems*, volume 33, pages 6111–6122. Curran Associates, Inc., 2020. 3
 - [50] Benjamin Ummenhofer, Lukas Prantl, Nils Thuerey, and Vladlen Koltun. Lagrangian fluid simulation with continuous convolutions. In *International Conference on Learning Representations*, 2020. 3
 - [51] Ricardo Vinuesa and Steven L Brunton. Enhancing computational fluid dynamics with machine learning. *Nature Computational Science*, 2(6):358–366, 2022. 3
 - [52] Peng Wang, Lingjie Liu, Yuan Liu, Christian Theobalt, Taku Komura, and Wenping Wang. Neus: Learning neural implicit surfaces by volume rendering for multi-view reconstruction. *arXiv preprint arXiv:2106.10689*, 2021. 2
 - [53] Maximilian Werhahn, You Xie, Mengyu Chu, and Nils Thuerey. A multi-pass gan for fluid flow super-resolution. *Proc. ACM Comput. Graph. Interact. Tech.*, 2(2), jul 2019. 3
 - [54] You Xie, Erik Franz, Mengyu Chu, and Nils Thuerey. tempogan: A temporally coherent, volumetric gan for super-resolution fluid flow. *ACM Transactions on Graphics (TOG)*, 37(4):95, 2018. 3
 - [55] Lior Yariv, Yoni Kasten, Dror Moran, Meirav Galun, Matan Atzmon, Basri Ronen, and Yaron Lipman. Multiview neural surface reconstruction by disentangling geometry and appearance. *Advances in Neural Information Processing Systems*, 33, 2020. 2
 - [56] Xiuming Zhang, Pratul P Srinivasan, Boyang Deng, Paul Debevec, William T Freeman, and Jonathan T Barron. Nerfactor: Neural factorization of shape and reflectance under an unknown illumination. *ACM Transactions on Graphics (TOG)*, 40(6):1–18, 2021. 2